ChemCatChem

ChemCatChem
Chemistry Europe
European Chemical Societies Publishing

RESEARCH ARTICLE OPEN ACCESS

Nanosecond Pulsed Microwave Plasma Torch for Continuous In-Line H_2O_2 Supply: A Path to Stable and Scalable Plasma-Driven Biocatalysis

Tim Dirks[1] | Mery Sheryll Hernandez Maya[2] | Davina Stoesser[1] | Sophia Tille[1] | Frank Hollmann[3] | Alexander Navarrete Munoz[2]

[1]Applied Microbiology, Faculty of Biology and Biotechnology, Ruhr University Bochum, Bochum, Germany | [2]Institute for Micro Process Engineering (IMVT), Karlsruhe Institute of Technology, Eggenstein-Leopoldshafen, Germany | [3]Department of Biotechnology, Delft University of Technology, Delft, The Netherlands

Correspondence: Tim Dirks (tim.dirks@rub.de)

Received: 14 January 2026 | **Revised:** 28 July 2026 | **Accepted:** 7 August 2026

Keywords: hydroxylation| immobilization| microwave plasma| peroxygenase| tandem plasma-biocatalysis

ABSTRACT

Plasma-driven H_2O_2 generation offers a potential sustainable route for biotransformations, but its application is hindered by challenges such as insufficient H_2O_2 production and enzyme degradation. This study establishes plasma-driven biocatalysis using a nanosecond pulsed microwave plasma torch (npMWPT), highlighting its unique advantages over previously applied sources. npMWPT-driven biocatalysis addresses insufficient plasma-generated H_2O_2 production by enabling continuous H_2O_2 supply while decoupling plasma treatment from enzymatic reactions. We investigated the effectiveness of npMWPT-driven biocatalysis using both immobilized and free recombinant unspecific peroxygenase from *Agrocybe aegerita* (r*Aae*UPO) to convert ABTS and ethylbenzene. For ABTS, immobilized r*Aae*UPO demonstrated reusability across five reaction cycles (turnover number TON 44,637 $\mu mol_{ABTS^{\bullet}}$ $\mu mol L^{-1}{}_{rAaeUPO}$). The decoupling of npMWPT-based H_2O_2 production resulted in a TON of 66,495 $\mu mol_{(R)\text{-1-PhOl}}$ $\mu mol L^{-1}{}_{rAaeUPO}$ with ethylbenzene for free r*Aae*UPO, outperforming the use of immobilized r*Aae*UPO for the first time in plasma-driven biocatalysis (TTN 22,116). Mixing optimization improved conversion rates, while observed enzyme inactivation under continuous operation revealed that H_2O_2 generation exceeded enzymatic consumption under the investigated conditions. The present study identifies supply-demand matching as the key optimization target for npMWPT-driven biocatalysis. This proof-of-principle work demonstrates the successful integration of spatially decoupled npMWPT H_2O_2 generation with peroxygenase-based biocatalysis and provides a basis for future process-controlled plasma-driven biocatalysis.

1 | Introduction

Peroxygenases, including the recombinant unspecific peroxygenase (r*Aae*UPO) from *Agrocybe aegerita* [1], are a class of heme-containing enzymes that catalyze various oxyfunctionalization reactions using hydrogen peroxide (H_2O_2), including stereoselective hydroxylations [2] and epoxidations [3, 4] that are challenging to achieve through conventional chemical methods. These characteristics make peroxygenases highly attractive for biocatalytic and industrial applications. Despite their potential, the industrial application of peroxygenases is limited by their sensitivity to H_2O_2, as the heme cofactor gets disrupted in a process called suicide inactivation [5–7]. Consequently, an in situ H_2O_2 generation strategy is essential to control H_2O_2 levels, thereby optimizing enzymatic activity while preventing inactivation [8].

Several in situ H_2O_2 generation strategies have been explored including electrochemistry [9–11], photocatalysis [12–14], or

enzyme cascades [2]. Each of these approaches offer distinct advantages and limitations regarding controllability, scalability, and compatibility for peroxygenase-based biocatalysis. Electrochemical H_2O_2 generation is particularly attractive due to its controllability, straightforward integration into flow systems, and the possibility of coupling H_2O_2 production directly to enzymatic catalysis. Electrochemical systems combined with peroxygenases have achieved high catalytic performances and turnover numbers (up to 400,000 $mol_{(R)\text{-1-PhOl}}$ $mol_{rAaeUPO}{}^{-1}$ based on the conversion of ethylbenzene), demonstrating the considerable potential of controlled H_2O_2 supply for selective oxyfunctionalization reactions [9]. However, limitations such as electrode stability, mass transfer limitations, and the requirement for conductive electrolytes can complicate process integration and long-term operational stability.

An emerging alternative involves atmospheric pressure plasmas, which produce H_2O_2 along with a variety of other reactive species. Beyond plasma-driven biocatalysis, the potential of plasma-generated reactive species for selective oxidation chemistry have also been investigated for catalytic oxidation reactions and environmental applications in plasma-liquid systems [15–17]. These characteristics also make plasma systems attractive for biocatalytic applications, where continuous plasma-based H_2O_2 generation can be used to drive peroxygenase-catalyzed reactions. In contrast to the addition of concentrated H_2O_2 stock solutions, plasma-based generation allows continuous and tunable H_2O_2 supply directly coupled to the biocatalytic reaction system. This may facilitate a more controlled adaptation of H_2O_2 supply to the enzymatic demand, which is particularly relevant for peroxygenases due to their sensitivity to excess H_2O_2. An initial study employed a dielectric barrier discharge (DBD) plasma source demonstrated the feasibility of using plasma-generated H_2O_2 to drive enzymatic reactions [18]. However, limitations such as enzyme inactivation by plasma-generated reactive species, primarily through residue modification (e.g. histidine and cysteine oxidation) [19–22] and peptide bond cleavage [23], or loss of cofactor heme [18] pose challenges.

To address these challenges, enzyme immobilization has been implemented as a method to increase enzyme stability under plasma conditions [24]. Immobilization on inert carrier materials spatially separates the enzyme from the most reactive plasma species, allowing especially short-lived reactive species to recombine, thereby reducing their impact on the enzyme. Additionally, immobilization facilitates the reuse of enzymes, enhancing the overall efficiency of the process [25–27]. Notably, the carrier material and immobilization chemistry affect both plasma stability and protection efficacy [28].

To date, three different plasma sources have been evaluated for their application in plasma-driven biocatalysis. While the general proof-of-principle was carried out using a dielectric barrier discharge (DBD) source from Cinogy (Germany), enzyme inactivation rates and limited treatable volumes (due to the geometry of the source) restrict its scalability [18]. Subsequent studies using plasma jet configurations showed improved results. Use of a micro-scale atmospheric pressure plasma jet (μAPPJ) in combination with immobilized r*Aae*UPO increased the achieved turnover number up to 36,415 $mol_{(R)\text{-1-PhOl}}$ $molL^{-1}{}_{rAaeUPO}$ and enabled treatment of larger volumes [29]. However, the application of the μAPPJ was constrained by limited water concentrations in the feed gas, since higher voltages are required for continuous plasma ignition, which could damage the electrodes of the plasma source [30]. The capillary plasma jet (CPJ) eliminated this limitation by introducing a capillary between the electrodes, which allows the application of higher input powers and thus higher water admixtures to enhance the plasma-induced H_2O_2 production [30–32]. CPJ-driven biocatalysis yielded a maximum turnover number of 174,209 $mol_{(R)\text{-1-PhOl}}$ $molL^{-1}{}_{rAaeUPO}$ using immobilized r*Aae*UPO [31]. Nevertheless, in these plasma setups the liquid is exposed to the plasma (DBD) or the effluent (μAPPJ, CPJ), destroying plasma-unstable substrates and products. The use of a plasma jet configuration also leads to significant evaporation of organic substrates due to the constant gas flow [29, 31]. In this study, we explored the integration of a nanosecond pulsed microwave plasma torch (npMWPT) for plasma-driven biocatalysis by producing in-line H_2O_2 in a preceding stage via continuous dropwise water flow treatment. In addition to avoiding plasma or effluent exposure of the reaction solution, this approach provides a continuously generated H_2O_2-containing stream whose concentration can potentially be adjusted through plasma power, pulse parameters, gas flow rate, and liquid flow rate. This enables future process-control strategies in which H_2O_2 generation is matched to enzymatic consumption, enabling a tunable and continuous co-substrate supply [31, 33]. Such controlled H_2O_2 delivery is particularly relevant for peroxygenase-catalyzed reactions, where both insufficient and excessive H_2O_2 concentrations can negatively affect catalytic performance and enzyme stability. Furthermore, the decentralized on-demand generation of H_2O_2 directly coupled to the biocatalytic process reduces the need for storage and handling of concentrated H_2O_2 solutions. In general, microwave plasmas offer several advantages, including electrodeless operation, the potential tuning of H_2O_2 generation and potentially higher energy efficiency than other types of plasmas [34]. However, common microwave plasma temperatures can exceed 4000 K [35], and such high temperatures are generally detrimental for H_2O_2, often leading to its decomposition and thereby limiting its overall production [33, 36]. Nonetheless, it has been previously reported that modulating the microwave signal in pulses of nanoseconds can sufficiently reduce the temperature in the plasma at atmospheric pressure compared to continues microwave applications [37]. Indeed, the nanosecond pulse microwave plasma method improved the continuous production of H_2O_2 and allowed tunable concentrations in the millimolar range (1–50 mmol L^{-1}), using water under argon plasma treatment [38]. This constantly produced and adjustable H_2O_2 can then drive the biocatalytic reaction.

2 | Results and Discussion

To enable effective integration of the npMWPT with biocatalysis, it was first necessary to establish plasma operating conditions that ensured consistent H_2O_2 production to drive the subsequent enzymatic biotransformation reactions. Thus, preliminary investigations aimed to select appropriate plasma operating parameters, including average input power, pulsation time, and gas and liquid flow rates. A constant set of microwave parameters was established, consisting of a pulsation duration (t_{on}) of 500 ns and interpulse time (t_{off}) of 1167 ns, corresponding to a duty cycle of 30%. The total argon gas flow rate was kept constant

TABLE 1 | Product formation and kinetic parameters of r*Aae*UPO catalyzed ABTS conversion using npMWPT-treated water as H_2O_2 source.

Substrate available (μmol)	5
Substrate converted (μmol)	2.28 ± 0.04
Conversion rate (μmol min^{-1})	1.14 ± 0.02
kcat (s^{-1})	380.31 ± 0.63
Turnover number (μmol_{ABTS^*} $\mu moL^{-1}{}_{rAaeUPO}$)	45,637.10 ± 76.26

at 8.7 L min^{-1}, and the water flow rate was held constant at 2.5 mL min^{-1}. Under these conditions, the specific energy input (SEI) was estimated at approximately 1.03 kJ $L^{-1}{}_{gas}$. Overall, the selected parameters yielded plasma-treated liquid containing H_2O_2 concentrations of 1.97 ± 0.09 mmol L^{-1}. The plasma-liquid treatment was operated continuously, and liquid samples were collected over a 4 h period of operation to verify the stability of the liquid product (more details are included in Table S1). The gas temperature was measured at around 2 cm away from the plasma-liquid reaction environment with values of 45°C ± 1. Additionally, all the experiments were carried out using a cooling coil downstream of the plasma zone, which further reduced the liquid product's temperature down to room temperature [38]. The optical emission spectroscopy analysis of the plasma-water interaction zone revealed the presence of OH (A-X) (306 to 315 nm), hydrogen Balmer lines Hα (656 nm), Hβ (485 nm), and Hγ (420 to 430 nm); and atomic oxygen lines (777 and 844 nm). The main species related to the formation of H_2O_2 are the OH and H species via electronic excitation and recombination reactions as supported by detailed OES analysis reported previously [38]. Moreover, in this qualitative spectroscopic analysis, no emission bands attributable to nitrogen-containing plasma species (315 – 380 nm [38]) were detected, which represents an advantage for enzymatic reactions. Figure S3 summarizes a representative OES spectrum for the selected experimental parameters. The OES analysis was primarily used as a qualitative tool to verify the reactive species present during the plasma-liquid interaction and to confirm the absence of undesired air or nitrogen related species that could negatively affect the subsequent enzymatic process. A systematic quantitative correlation between plasma-generated species and enzymatic performance would require variation of plasma operating conditions and analysis of the resulting OES trends, which was beyond the scope of the present proof-of-concept study focused on in-line continuous plasma-driven H_2O_2 supply for biocatalysis. A more detailed and quantitative OES analysis under varying plasma conditions for enzymatic processes will be addressed in future studies.

Following the selection of plasma parameters to reliably produce H_2O_2, the next step consisted of integrating the plasma-treated liquid with the enzymatic conversion reaction. Initially, a decoupled experimental setup was chosen to verify the general integration of the npMWPT in the process of plasma-driven biocatalysis. The conversion of the plasma-unstable substrate ABTS by the r*Aae*UPO via its peroxidase activity (one-electron transfer reaction) was analyzed using a continuous flow of plasma-treated water as a H_2O_2 source over a reaction time of 2 min (Table 1). Of the 5 μmol ABTS present in the reaction, 45.6% (2.28 μmol) were converted with a conversion rate of 1.14 μmol min^{-1}. As a control to assess whether potentially generated plasma species other than H_2O_2 had an adverse influence on the reaction, the experiment was repeated but replacing the plasma-treated water with an H_2O_2 solution containing the same amount of co-substrate. Product formation of 2.11 μmol (± 0.06) was confirmed again, which was at the same level as achieved using the npMWPT. This suggests that H_2O_2 is in fact the dominant long-lived species in plasma-treated water, as no reduction in product formation due to side reactions involving other plasma species negatively affecting enzyme activity could be detected. This decoupled proof-of-principle experiment resulted in a turnover number of 45,637.10 μmol_{ABTS^*} $\mu moL^{-1}{}_{rAaeUPO}$, already exceeding the maximum reported μAPPJ-driven biocatalysis turnover value [29]. However, this turnover number was achieved based on the conversion of the substrate ethylbenzene, whose turnover represents a two-electron transfer reaction (peroxygenase activity). Nevertheless, the achieved ABTS conversion demonstrated, for the first time, that plasma-driven biocatalysis is workable with plasma-unstable substrates using H_2O_2 generated by the npMWPT.

The process of enzyme immobilization is a key element of the established plasma-driven biocatalysis, since it has generally been shown that proteins are protected better against plasma-induced inactivation when immobilized [24, 28]. Thus, the biocatalytic efficiency has also been substantially increased by extending the lifetime of the enzymes in plasma-driven biocatalysis [29, 31]. Additionally, immobilization allows the separation of enzymes from the reaction mixture, reducing the contamination of the product by enzymes, while immobilized enzymes can be reused for multiple reaction cycles without additional purification and recycling steps [25–27]. The potential utilization of immobilized r*Aae*UPO with the npMWPT was tested by transferring enzyme-loaded beads in a rotating bed reactor and adding 1 mL of ABTS substrate solution. A continuous flow of plasma-treated water was then supplied for 2 min and the absorbance was measured every 30 s to determine the product formation (scheme of the experimental setup is displayed in Figure S2a). To confirm the previously stated benefit of using the immobilized enzymes in multiple reaction cycles with the npMWPT in plasma-driven biocatalysis, the ABTS conversion was repeated for a total of five reaction cycles with the same set of enzyme-loaded beads (Figure 1).

During the first reaction cycle, 1.87 μmol ABTS* was formed in 2 min at a rate of 0.93 μmol min^{-1}, representing the highest conversion rate of all five cycles. Subsequently, the product formation was slightly reduced (0.63 μmol min^{-1}), while no significant decrease in conversion rate was observed after the five cycles. Consequently, the process could presumably be continued for further cycles with the same set of enzyme-loaded beads in order to further increase the biocatalytic efficiency. However, analysis of the residual enzyme activity after biocatalysis revealed a substantial inactivation, showing only a residual activity of 10.42% (Table S2). The apparent loss of activity was presumably promoted by the constant incubation of the enzymes in excess H_2O_2 conditions.

Within the five reaction cycles (total reaction time of 600 s), it was possible to build up an accumulated product amount of 6.89 ± 1.16 μmol with a linear increase of 0.66 μmol_{ABTS^*} min^{-1} (Figure 1b). This resulted in a turnover number of

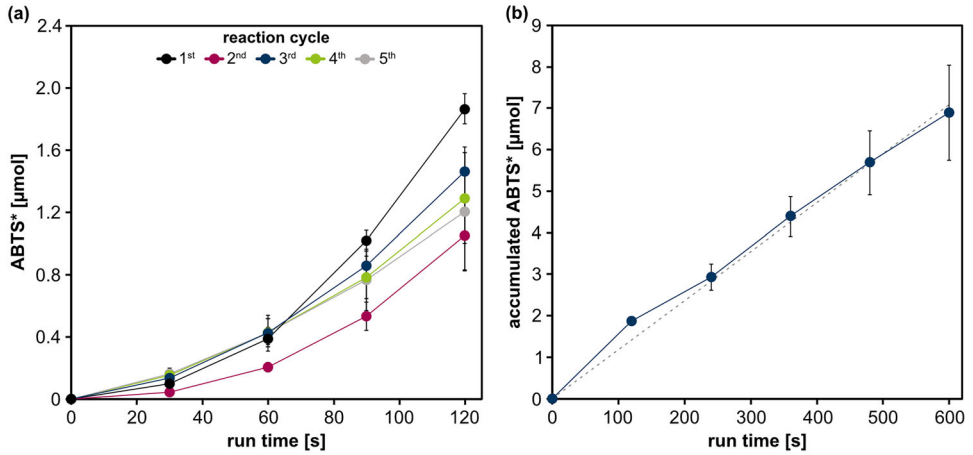

FIGURE 1 | Substrate (ABTS) conversion performing plasma-driven biocatalysis using immobilized r*Aae*UPO with npMWPT. (a) Conversion of ABTS using immobilized r*Aae*UPO was tested by transferring 100 mg protein-loaded beads to a rotating bed reactor, which was placed in a vessel filled with 1 mL ABTS (5 mmol L^{-1}) dissolved in 100 mmol L^{-1} citrate buffer (pH 5). Plasma-treated water was added at a flow rate of 2.5 mL min^{-1} for 2 min, while the absorbance was measured every 30 s at 405 nm. To prove the reusability of the r*Aae*UPO-loaded beads, the whole reaction solution was withdrawn from the vessel and the reaction cycle was repeated (total cycle amount of five). The total product amount was calculated under consideration of the introduced dilution factor and based on the millimolar extinction coefficient (ε = 36.8 mmol L^{-1} cm^{-1}). (b) Accumulation of formed product (ABTS* in µmol) over the total run time of 600 s in five reaction cycles. Means and standard deviations reflect three independent experiments. Standard deviations that are not visible were below 0.02 µmol (a) or 0.1 µmol (b).

44,125.89 μmol_{ABTS*} $\mu molL^{-1}{}_{rAaeUPO}$, which was at a very similar level to the turnover of ABTS using the free enzyme (45,637.10 μmol_{ABTS*} $\mu molL^{-1}{}_{rAaeUPO}$). In control experiments, in which the flow of plasma-treated water was replaced with co-substrate solutions (1.97 mmol L^{-1}), the same level of product formation was confirmed (8.28 µmol ± 1.23, Figure S4). In addition, the residual activity of the enzyme-loaded beads after the control experiments was 7.2%, which was comparable to the residual activity observed after npMWPT-driven reactions. This demonstrates that no negative influence on the catalytic reaction occurred due to potential other plasma-generated species, and that product formation is attributable mainly to the enzyme-driven reaction involving the co-substrate. Furthermore, the comparable residual activities observed after both plasma-based and control reactions strongly indicate that the pronounced enzyme inactivation was primarily caused by the excess H_2O_2 conditions rather than by additional plasma-generated reactive species. Overall, we conclude that biocatalysis proceeds at a slower conversion rate when the immobilized enzyme is introduced (catalytic constants: 380 s^{-1} free r*Aae*UPO; 70.42 s^{-1} immobilized r*Aae*UPO). It has been reported previously that immobilization may lead to a reduction in the general activity of enzymes [18]. However, the immobilization-induced increase in enzyme stability and especially the increase of their lifetime under plasma treatment conditions led to a positive effect on the biocatalytic efficiency in previously established plasma-driven biocatalysis setups [18, 29, 31]. In this study, the same turnover number was achieved in just one-fifth of the reaction time by using the free enzyme, showing no advantage for using immobilized r*Aae*UPO in terms of efficiency in npMWPT-driven biocatalysis. The rather indirect treatment of the enzyme with the npMWPT results in a low inactivation level of the free enzyme. Plasma-induced inactivation and especially degradation of proteins is primarily caused by short-lived and highly reactive species (e.g. OH radicals) [23, 28]. Since r*Aae*UPO comes only into contact with the plasma-treated water during npMWPT-driven biocatalysis, the short-lived and highly reactive plasma species presumably have already reacted before reaching the enzyme. Consequently, their detrimental effect on the activity of the free enzyme is likely negligible, thereby diminishing the efficiency-enhancing effect typically associated with enzyme immobilization. This interpretation is further supported by control experiments in which the plasma-treated water supply was replaced by co-substrate solutions containing identical concentrations of hydrogen peroxide (1.97 mmol L^{-1}). Under these conditions, comparable product formation was observed (8.28 µmol ± 1.23, Figure S4). These results show that plasma-generated by-products do not measurably interfere with the catalytic reaction and confirm that product formation originates from the enzyme-catalyzed conversion driven by the plasma-supplied co-substrate.

After confirmation of the general feasibility of utilizing npMWPT in plasma-driven biocatalysis on the basis of ABTS conversion employing the peroxidase activity of r*Aae*UPO, we aimed to transfer the process to the model reaction for the peroxygenase activity of the enzyme, namely the conversion of ethylbenzene to (*R*)-1-phenylethanol. As previously for ABTS, a proof-of-principle approach was initially chosen by adding 50 mmol L^{-1} ethylbenzene and r*Aae*UPO (50 or 100 nmol L^{-1}) to 1.5 mL npMWPT-treated water. After 10 min incubation under constant mixing to assure sufficient exposure of the enzyme to the organic substrate, the product conversion was analyzed (Figure 2).

The substrate ethylbenzene was available in excess together with a total of 3 µmol plasma-produced co-substrate H_2O_2, of which approx. 50% (1.43 µmol) was converted into the product (*R*)-1-PhOl when applying 0.075 nmol r*Aae*UPO. With the aim of achieving higher conversions, the experiment was repeated with twice the amount of enzyme (0.15 nmol), resulting in the production of 2.88 µmol (*R*)-1-PhOl converting almost the entire amount of co-substrate. The endpoint measurement

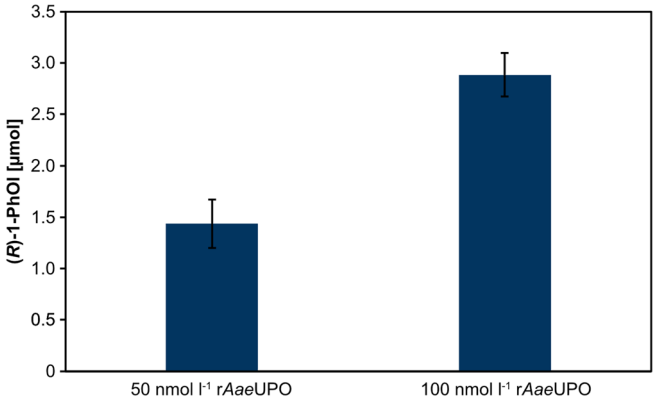

FIGURE 2 | Ethylbenzene conversion using npMWPT-treated water in combination with free r*Aae*UPO. Plasma-treated water (1.5 mL) was mixed with 50 mmol L^{-1} ethylbenzene and 50 or 100 nmol L^{-1} (0.075 or 0.15 nmol) free r*Aae*UPO. After 10 min incubation under rapid mixing, 150 µl sample was withdrawn for gas chromatography (GC) analysis. Means and standard deviations represent three independent experiments.

TABLE 2 | Product formation and kinetic parameters of r*Aae*UPO (0.15 nmol) catalyzed ethylbenzene conversion using npMWPT-treated water as H_2O_2 source.

Substrate available (µmol)	**3**
Substrate converted (µmol)	2.88 ± 0.22
Conversion rate (µmol min^{-1})	0.28 ± 0.02
k_{cat} (s^{-1})	32.07 ± 2.46
Turnover number ($\mu mol_{(R)\text{-1-PhOl}}\ \mu mol L^{-1}{}_{rAaeUPO}$)	19,239.50 ± 1,479.32

of the product formation resulted in a conversion rate of 0.288 $\mu mol_{(R)\text{-1-PhOl}}\ min^{-1}$, a catalytic constant of 32.07 s^{-1}, and a turnover number of 19,239 $\mu mol_{(R)\text{-1-PhOl}}\ \mu mol L^{-1}{}_{rAaeUPO}$ (Table 2).

To verify that the observed product formation was attributable to the enzymatic reaction driven by hydrogen peroxide, a control experiment was performed in which the npMWPT-treated water was replaced by an H_2O_2 solution at equivalent concentrations while maintaining the same enzyme concentration (0.15 nmol r*Aae*UPO). Under these conditions, a comparable product concentration was obtained (2.71 µmol ± 0.47), confirming that other potentially generated plasma species did not significantly influence the catalytic reaction.

After confirming the proof-of-principle for the implementation of npMWPT in plasma-driven biocatalysis based on the decoupled setup for the conversion of the organic substrate, we set out to analyze the reaction under continuous supply of the co-substrate utilizing the free enzyme (scheme of the experimental setup is displayed in Figure S2a). To this end, r*Aae*UPO was placed in an ethylbenzene buffer mix and a constant flow of plasma-produced H_2O_2 was provided, which was stopped after 2 min. Immediately after the two minutes, a first sample was withdrawn ('after reaction'). The reaction solution was then incubated for 10 min to allow conversion of residual H_2O_2 ('after incubation'). In an initial attempt, the reaction mixture was mixed with the aid of magnetic

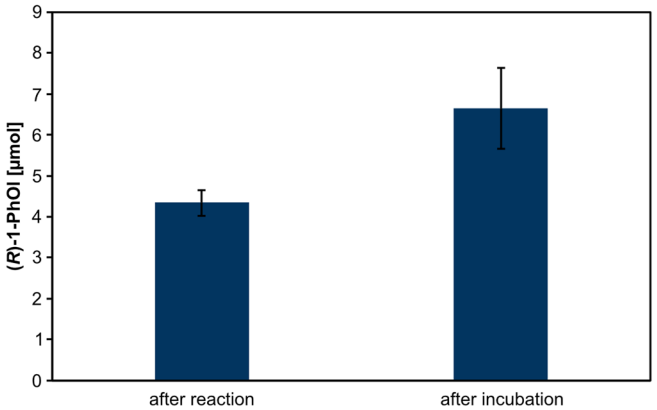

FIGURE 3 | Ethylbenzene conversion using continuous flow of npMWPT-treated water in combination with free r*Aae*UPO. Ethylbenzene (50 mmol L^{-1}) was mixed with free r*Aae*UPO (0.1 nmol) in a total volume of 1 mL potassium phosphate buffer (100 mmol L^{-1}, pH 7). Continuous flow of npMWPT-treated water at a flow rate of 2.5 mL min^{-1} was added over a time frame of 2 min, while the solution was mixed using an empty rotating bed reactor at 900 rpm. After 2 min, the flow of plasma-treated water was stopped. Samples (150 µl) were withdrawn for GC analysis directly after 2 min ('after reaction') and after further 10 min incubation ('after incubation') to allow conversion of residual H_2O_2. Means and standard deviations reflect three independent experiments.

stirring to ensure that the poorly water-soluble ethylbenzene had sufficient interactions with the enzyme (Figure S5). This resulted in the formation of only 2.22 µmol (after reaction) or 2.72 µmol (after incubation) (*R*)-1-PhOl, although 10 µmol co-substrate H_2O_2 was present. To test whether the low conversion (~ 25%) was due to insufficient mixing, the experiment was repeated using a rotating bed reactor, which was not filled with immobilized enzymes but was only used for improved mixing (Figure 3). Directly after 2 min, 4.33 µmol (*R*)-1-PhOl was formed, showing already improved substrate conversion. After further incubation, apparent residual H_2O_2 was converted resulting in an increased product formation of 6.65 µmol (*R*)-1-PhOl. Comparable product concentrations were obtained in control experiments in which the plasma-treated water supply was replaced by co-substrate solutions with equivalent concentrations (1.97 mmol L^{-1}), yielding 3.95 µmol ± 0.34 ('after reaction') and 6.21 µmol ± 0.74 ('after incubation') (*R*)-1-PhOl. Employing the constant flow of plasma-produced H_2O_2 with free r*Aae*UPO, a turnover number of 66,495.06 $\mu mol_{(R)\text{-1-PhOl}}\ \mu mol L^{-1}{}_{rAaeUPO}$ was achieved. In contrast to the ABTS-based turnover numbers, this value is directly comparable with previous plasma-driven biocatalysis setups since it is based on the same catalyzed reaction. Using the npMWPT-driven biocatalysis, a higher turnover number was achieved compared to the µAPPJ [29]. A 2.5-fold higher turnover number was realized using the capillary plasma jet in an 11 h catalysis [31]. Interestingly, immobilized r*Aae*UPO was used in the other two plasma jet-based processes to achieve the respective turnover numbers through protection of the enzyme, whereas in this study promising biocatalytic efficiencies were achieved for the first time employing free r*Aae*UPO in combination with online plasma-based H_2O_2 production. In addition, higher turnover numbers could previously only be achieved with longer reaction times, which especially increases gas consumption and thereby costs [31]. The improved conversion (~ 65%) by introducing the

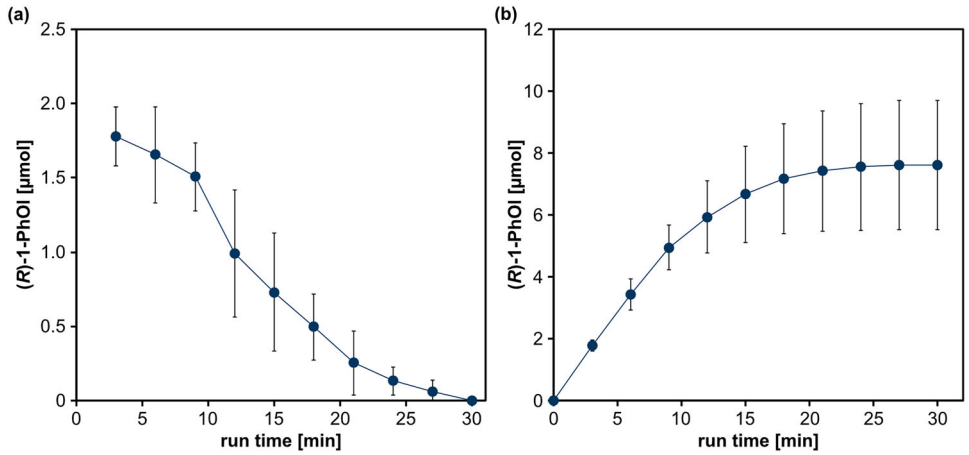

FIGURE 4 | Substrate (ethylbenzene) conversion performing plasma-driven biocatalysis using immobilized r*Aae*UPO with npMWPT. (a,b) Conversion of ethylbenzene with immobilized r*Aae*UPO was analyzed by loading 200 mg enzyme-loaded beads into a rotating bed reactor. The flow of substrate (100 mmol L^{-1} ethylbenzene in 100 mmol L^{-1} potassium phosphate buffer, pH 7) was combined with the continuous flow of the plasma-treated water (total flow rate of 5 mL min^{-1}) and continuously supplied to the reaction vessel with the rotating bed reactor for a total run time of 30 min. Every 45 s, samples of 3.75 mL were withdrawn to prevent overflowing of the reaction vessel, while four samples were pooled in one reaction tube (total volume of 15 mL). (a) To analyze product formation in the respective 3 min time frame, 150 µl sample was withdrawn for GC measurement. (b) Accumulation of (*R*)-1-PhOl performing plasma-driven biocatalysis calculated by addition of all measured (*R*)-1-PhOl amounts during the 30 min biocatalysis. Means and standard deviations represent three independent experiments.

empty rotating bed reactor for better mixing also highlights the importance of sufficient mixing when working with the organic substrate ethylbenzene. This has previously been discussed in the context of plasma-driven biocatalysis in association with substrate limitation, as the jet configurations resulted in a rather high level of substrate evaporation due to the poor solubility of ethylbenzene [29, 31]. However, this limitation may be overcome with the npMWPT-driven biocatalysis by introducing a suitable mixing method.

For conversion of ABTS, it was previously demonstrated that immobilization did not provide any advantages in the biocatalytic conversion efficiency. Nevertheless, the general implementation and optimization of plasma-driven biocatalysis using immobilized enzymes is advantageous for future process costs and the separation of the product from the enzyme. Hence, the ethylbenzene conversion was also investigated using immobilized r*Aae*UPO. A major challenge was the poor solubility of ethylbenzene and thus the need for sufficient mixing. Once again, a rotating bed reactor was used for this purpose, but this time it was filled with enzyme-loaded beads. In addition, a second pump was introduced to ensure a constant flow of ethylbenzene. This flow was combined with the flow of npMWPT-treated water and was supplied as a combined flow to the reaction batch containing the rotating bed reactor, ensuring that both substrate and co-substrate were supplied to the enzyme at the same time (scheme of the experimental setup is displayed in Figure S2b). Plasma-driven biocatalysis was carried out over a period of 30 min, while product formation was analyzed every 3 min (Figure 4a). Within the first 9 min, the product formation was constant (0.5 – 0.59 $\mu mol_{(R)\text{-1-PhOl}}$ min^{-1}). Subsequently, product formation decreased over time, resulting in a conversion rate of 0.08 $\mu mol_{(R)\text{-1-PhOl}}$ min^{-1} after 24 min. At the last measurement point (27 – 30 min), no product was detected. The apparent enzymatic inactivation was confirmed by testing for residual activity of the immobilized enzymes. In total, 7.61 $\mu mol_{(R)\text{-1-PhOl}}$ were produced using a continuous supply of plasma-treated water and substrate (Figure 4b), resulting in a total turnover number of 22,116.49 $\mu mol_{(R)\text{-1-PhOl}}$ $\mu molL^{-1}{}_{r\mathit{Aae}UPO}$ (Table S3). Control experiments were performed under otherwise identical conditions, replacing the plasma-treated water with H_2O_2 solutions supplying an equivalent amount of co-substrate. Comparable product formation and reaction kinetics were observed (Figure S6).

The comparatively low total turnover number achieved clearly highlights the limitations as well as the advantages of npMWPT-driven biocatalysis. The initial conversion rates (up to 9 min) were relatively constant. However, the product formation proceeded at a rate of 0.55 µmol min^{-1}, while theoretically 5 µmol min^{-1} H_2O_2 were supplied. Thus, a 10-fold H_2O_2 excess affected the r*Aae*UPO, which potentially leads to the rather severe inactivation. Due to the increasing inactivation, the H_2O_2 excess also increases further during biocatalysis, resulting in complete inactivation of the enzyme after 30 min and thus comparatively low product formation. A real-time quantification of H_2O_2 concentrations during biocatalysis was not performed in the present study. Therefore, the temporal evolution of local H_2O_2 concentrations during enzymatic turnover and their quantitative correlation with enzyme inactivation could not be resolved in detail. Nevertheless, the comparable residual enzyme activities and product formations observed in control experiments (Figure S6) using externally prepared H_2O_2 solutions strongly indicate that the observed enzyme inactivation was primarily associated with excess H_2O_2 exposure rather than additional plasma-generated reactive species. The reactor concept thus needs to be adapted, especially on the enzymatic side, so that H_2O_2 excess is prevented by applying increased enzyme loading for faster conversions. As this is only partially possible in our present setup due to the geometries of the rotating bed reactor, this requires future optimization. Generally, the implementation of a different reactor

concept is conceivable. A column-based reactor setup instead of a rotating bed reactor may be a suitable option, as the investigated plasma source already provides a continuous flow of plasma-treated water that could be coupled to the enzyme-filled column [39–41]. Such a column reactor setup combined with a continuous flow of H_2O_2 stock solutions has already been tested with the unspecific peroxygenase from *Agrocybe aegerita*, resulting in promising results [42].

This limitation shows that the npMWPT shifts the process bottleneck away from the H_2O_2 generation, which is no longer limiting, to the controlled co-substrate utilization by the enzymatic reactor. Therefore, future adjustments should focus on optimizing the reactor design to ensure the efficient conversion of the now abundantly available co-substrate H_2O_2. The npMWPT setup demonstrates that continuous plasma-generated H_2O_2 supply can also be accomplished using a nanosecond pulsed microwave plasma source coupled with peroxygenase-driven biocatalysis. In contrast to previously investigated plasma configurations involving direct plasma or plasma-effluent exposure of the reaction mixture [29, 31], the spatial separation of H_2O_2 generation and enzymatic conversion in the present setup may provide advantages regarding substrate compatibility and reduced exposure of the enzyme to short-lived reactive plasma species. The novelty of the npMWPT-based co-substrate production is thus not the general plasma-based generation of H_2O_2 itself, but the implementation of a nanosecond pulsed microwave plasma source as a continuous in-line H_2O_2 supply source spatially decoupled from the enzymatic reaction environment. While the present study primarily focused on demonstrating the general compatibility of the npMWPT concept with plasma-driven biocatalysis, the plasma source inherently offers the possibility to tune species production through adjustment of plasma operating parameters such as power input, pulse conditions, and gas or liquid flow rates. Future studies may therefore exploit this tunability to dynamically adapt H_2O_2 generation rates to the enzymatic demand to improve catalyst stability and overall process efficiency. While continuous dosing of externally prepared H_2O_2 solutions remains a potential strategy for peroxygenase catalysis, it relies on the continuous consumption of a pre-prepared feedstock. In contrast, plasma-based H_2O_2 generation provides the opportunity to continuously regenerate the co-substrate directly within the process, thereby opening the perspective of future recirculation-based reactor concepts in which the reaction medium is continuously recycled through the plasma unit. Such concepts could, in principle, maintain an approximately constant reaction volume while reducing buffer consumption, product dilution, and downstream wastewater generation.

Importantly, the presented npMWPT architecture extends this concept further by spatially separating plasma treatment from the enzymatic reactor. Unlike previously reported plasma-driven biocatalysis systems, this architecture combines continuous plasma-based H_2O_2 generation with the ability to process plasma-sensitive substrates while minimizing direct exposure of the enzyme to short-lived reactive plasma species. Consequently, the process is not limited by the compatibility of substrates or biocatalysts with the plasma itself but rather by the efficient utilization of the generated H_2O_2. This shift in the process bottleneck highlights that the proposed architecture decouples H_2O_2 generation from plasma compatibility constraints and instead places the focus on reactor engineering and matching co-substrate generation with enzymatic consumption.

3 | Conclusion

In conclusion, this study demonstrates the proof-of-principle of npMWPT-driven tandem biocatalysis by integrating continuous plasma-based H_2O_2 generation in-line with peroxygenase-catalyzed reactions. The spatial decoupling of H_2O_2 generation from the enzymatic reaction enabled the conversion of plasma-sensitive substrates such as ABTS and allowed ethylbenzene oxyfunctionalization using free r*Aae*UPO. Notably, under the conditions tested, free r*Aae*UPO outperformed immobilized r*Aae*UPO during short reaction times, indicating that the indirect exposure of the enzyme to plasma-treated water can reduce the need for immobilization as a protective strategy. At the same time, the continuous-flow experiments with immobilized r*Aae*UPO revealed that enzyme inactivation was mainly caused by excess H_2O_2. Therefore, further development should focus on reactor design, enzyme loading, mixing, and dynamic matching of H_2O_2 generation with enzymatic demand. This proof-of-concept work establishes a spatially decoupled, continuous npMWPT-based H_2O_2 supply architecture for plasma-driven biocatalysis, demonstrating the compatibility of on-demand and in-line plasma-generated H_2O_2 with peroxygenase catalysis while enabling independent optimization of plasma and biocatalytic processes. The comparable conversions obtained with plasma-treated water and externally prepared H_2O_2 solutions highlight that H_2O_2 supply-demand matching is the key design criteria for future reactor optimization. Future developments should additionally focus on constant-volume operation with controlled H_2O_2 delivery while maintaining separation of the reaction medium from the plasma, considering parameters such as H_2O_2 utilization, catalyst lifetime, space-time yield, and energy and argon demand.

4 | Experimental Section

4.1 | Plasma Source

The plasma-water reaction system consists of a coaxial plasma torch reactor (Heuermann HF–Technik GmbH) connected to a solid-state microwave source (TRUMPF Hüttinger Microwave). The gas flow was fed into the torch using mass flow controllers (MFC, Vögtlin Instruments), and the liquid was fed via a 1.8 mm (o.d.) stainless steel tube connected to a water pump (1HM, Eldex, USA). A thermocouple was located approx. 2 cm away from the plasma zone to follow the temperature of the reaction environment. The quenching of the plasma zone was achieved using a metallic loop stainless steel tubing (1/8" i.d.) placed below the plasma-liquid interaction zone. The liquid product was collected downstream using a three-way valve that allows to take a specific amount of sample when required. An optical fiber connected to a UV–vis detector (USB2000, Ocean Optics, USA) served as an optical emission spectrometer (OES), enabling real-time monitoring of species during the plasma-water interaction. The OES was primarily used to identify the species present in the plasma phase and to confirm the absence of undesired nitrogen- or air-related species that could interfere with the subsequent

enzymatic process. Due to the limited spectral resolution of the system, quantitative analysis of the detected species was not possible. Since all enzymatic experiments were performed under constant plasma operating conditions, the plasma chemistry remained essentially unchanged throughout the study. A schematic representation of the experimental set up is shown in Figure S1. The main parameters to establish during pulsed operation of the microwave source are the time of active pulse (t_{on}) and the time of inactive pulse (t_{off}), where the sum of both represents the total pulse period. The fraction of t_{on} over the total pulse period represents the duty cycle (DC) (Equation 1). Furthermore, the specific energy input (SEI) used for the reaction can be estimated through Equation 2.

$$\frac{t\_on}{t\_on + t\_off} = \text{duty cycle} \quad (1)$$

$$SEI\,(kJ/L) = \frac{power\,(kW)}{gas\ flow\ rate\,(L/s)} \quad (2)$$

4.2 | H_2O_2 Measurement

The H_2O_2 concentration was measured using the common titanium oxysulfate ($TiOSO_4$) method, where the absorption intensity of the yellow-colored pertitanic acid complex (H_2TiO_4) at 407 nm is proportional to the reacted H_2O_2 [43]. For preparing a sample, a 1:1 mixture of the plasma-treated liquid and a $TiOSO_4$ solution (0.156 M) was prepared, and 5 mL of deionized water was added. Further details can be found in [44].

4.3 | Enzyme Preparation and Immobilization

r*Aae*UPO was purified as described previously [45]. For immobilization, amino (HA403 M) functionalized beads (Resindion, Italy) were used. In a suitable vessel, 500 mg beads were weighed and washed thrice with 5 mL potassium phosphate buffer (100 mmol L^{-1}, pH 7). Carrier materials were incubated for 3 h in the presence of 0.5 % (w/v) glutaraldehyde in a total volume of 5 mL potassium phosphate buffer (100 mmol L^{-1}, pH 7). After incubation, beads were washed thrice with potassium phosphate buffer to remove the glutaraldehyde. Finally, enzyme (2 nmol) was added, and immobilization was carried out overnight at 8°C with overhead shaking.

4.4 | Binding Efficiency

Enzyme binding efficiency was evaluated by measuring residual enzyme activity in the supernatant after immobilization. Using 2,2'-azino-bis(3-ethylbenzothiazoline-6-sulfonic acid) (ABTS) as substrate, either r*Aae*UPO (2 nmol) or supernatant after immobilization was added to 100 mmol L^{-1}sodium citrate buffer (pH 5) containing ABTS (5 mmol L^{-1}). An equivalent volume of H_2O_2 (2 mmol L^{-1}) was added to initiate the reaction, while product formation was monitored at 405 nm using a microplate reader (Biotek Epoch, Germany). Final concentrations were 2.5 mmol L^{-1} ABTS, 1 mmol L^{-1} H_2O_2, and 50 mmol L^{-1} citrate. Unimmobilized r*Aae*UPO served as a control.

4.5 | Enzyme Activity Assays

Proof-of-principle of the potential compatibility of the plasma-generated H_2O_2 with enzymatic conversions was carried out with different configurations, varying the substrate and the enzyme immobilization status.

4.5.1 | ABTS Conversion Using Free r*Aae*UPO

ABTS (5 mmol L^{-1}) was mixed with 50 nmol L^{-1} (0.05 nmol) free r*Aae*UPO in 100 mmol L^{-1} sodium citrate buffer (pH 5) and a total volume of 1 mL. Plasma-treated water was added at a flow rate of 2.5 mL min^{-1} for 2 min and endpoint absorbance was measured at 405 nm using a microplate reader (Biotek Epoch). For control experiments, H_2O_2 feedstock (1.97 mmol L^{-1}) was added at a flow rate of 2.5 mL min^{-1} for 2 min using a peristaltic pump (LabN1-II/AMC4(10) pump, Drifton, Denmark) instead of plasma-treated water. Based on the millimolar extinction coefficient of ABTS (ε = 36.8 mmol L^{-1} cm^{-1}), the total product amount was calculated under consideration of the introduced dilution factor.

4.5.2 | Decoupled Continuous ABTS Conversion Using Immobilized r*Aae*UPO

Conversion of ABTS using immobilized r*Aae*UPO was tested by transferring 100 mg protein-loaded beads to a rotating bed reactor (built in-house, dimensions: ∅ 2 cm · 0.7 cm), which was placed in a vessel filled with 1 mL ABTS (5 mmol L^{-1}) dissolved in 100 mmol L^{-1} citrate buffer (pH 5). Plasma-treated water was added at a flow rate of 2.5 mL min^{-1} for 2 min with absorbance measured every 30 s at 405 nm using a microplate reader (Biotek Epoch) (Figure S2a). To prove the reusability of the r*Aae*UPO-loaded beads, the whole reaction solution was withdrawn from the vessel and replenished, repeating the reaction with the same set of beads for a total of five cycles. For control experiments, H_2O_2 feedstock (1.97 mmol L^{-1}) was added at a flow rate of 2.5 mL min^{-1} for 2 min using a peristaltic pump (LabN1-II/AMC4(10) pump, Drifton) instead of plasma-treated water. The total product amount was calculated considering the introduced dilution factor and based on the millimolar extinction coefficient (ε = 36.8 mmol L^{-1} cm^{-1}). Residual activity of protein-loaded beads was checked by recovering the beads from the rotating bed reactor and washing them thrice with potassium phosphate buffer. Enzyme activity was determined as described for the binding efficiency analysis but in a total volume of 1 mL using 10 µl beads. Samples were shaken during turnover to ensure sufficient substrate supply. Every 2 min over a total of 10 min reaction time, aliquots of 100 µl were removed and measured using a microplate reader (Biotek Epoch) at a wavelength of 405 nm. Enzyme activity was calculated based on the linear slope of the kinetic. Untreated r*Aae*UPO-loaded beads served as a control for 100% residual enzyme activity.

4.5.3 | Ethylbenzene Conversion Using Free r*Aae*UPO

Plasma-driven biocatalysis converting ethylbenzene as substrate was initially evaluated using 1.5 mL plasma-treated water, which was mixed with 50 mmol L^{-1} ethylbenzene and 50 or 100 nmol L^{-1} (0.075 or 0.15 nmol) free r*Aae*UPO. After 10 min incubation

with vigorous mixing, 150 µl samples were withdrawn for gas chromatography (GC) analysis. As a control, 1.5 mL H_2O_2 solution (1.97 mmol L^{-1}) was mixed with 50 mmol L^{-1} ethylbenzene and 100 nmol L^{-1} free r*Aae*UPO.

4.5.4 | Decoupled Continuous Ethylbenzene Conversion Using Free r*Aae*UPO

For decoupled continuous-flow conversion of ethylbenzene, 50 mmol L^{-1} ethylbenzene was mixed with 100 nmol L^{-1} (0.1 nmol) free r*Aae*UPO in a total volume of 1 mL potassium phosphate buffer (100 mmol L^{-1}, pH 7). Plasma-treated water was continuously added at a flow rate of 2.5 mL min^{-1} for 2 min. The solution was mixed using a magnetic stirrer or an empty rotating bed reactor at 900 rpm. After 2 min, the flow of plasma-treated water was stopped. Samples (150 µl) were withdrawn for GC analysis directly after 2 min and after further 10 min incubation to allow conversion of residual H_2O_2 (Figure S2a). For control experiments, H_2O_2 feedstock (1.97 mmol L^{-1}) was added at a flow rate of 2.5 mL min^{-1} for 2 min using a peristaltic pump (LabN1-II/AMC4(10) pump, Drifton) instead of plasma-treated water.

4.5.5 | Coupled Continuous Ethylbenzene Conversion Using Immobilized r*Aae*UPO

Conversion of ethylbenzene using immobilized r*Aae*UPO was investigated by transferring 200 mg enzyme-loaded beads to the previously described rotating bed reactor. A substrate vessel was prepared containing 100 mmol L^{-1} ethylbenzene in potassium phosphate buffer (100 mmol L^{-1}, pH 7) and combined with the continuous flow of plasma-treated water. The combined flow of substrate and plasma-treated water (flow rate of 5 mL min^{-1}) was added to the reaction vessel containing the rotating bed reactor for a total run time of 30 min (Figure S2b). Every 45 s, samples of 3.75 mL were withdrawn to prevent overflow of the reaction vessel, while four samples were pooled in one reaction tube (total volume of 15 mL). To analyze product formation in the respective 3 min time frame, 150 µl samples were withdrawn for GC measurement. After 30 min of biocatalysis, residual activity of protein-loaded beads was determined as described previously for the ABTS conversion. As a control, the same experiment was repeated substituting the plasma-treated water flow with a bulk co-substrate solution (1.97 mmol L^{-1}) at a flow rate of 2.5 mL min^{-1} using a peristaltic pump (LabN1-II/AMC4(10) pump, Drifton).

4.6 | Analysis of (*R*)-1-PhOl

Samples of 150 µl were withdrawn and mixed with the same volume of ethyl acetate containing 2 mmol L^{-1} 1-octanol as internal standard. The organic phase was transferred to a new vial, dried with $MgSO_4$ and analyzed by gas chromatography (Shimadzu GC 2010 system equipped with Hydrodex β-6TBDM column, Macherey–Nagel, Germany). Samples were analyzed following an isothermal program (120°C, 11 min). Concentrations were determined based on a calibration curve that used racemic 1-PhOl.

Author Contributions

Tim Dirks: conceptualization, investigation, writing – original draft, writing – review and editing, visualization, validation, methodology, formal analysis, funding acquisition. **Mery Sheryll Hernandez Maya**: conceptualization, investigation, writing – original draft, formal analysis. **Davina Stoesser**: investigation. **Sophia Tille**: investigation. **Frank Hollmann**: resources, writing – review and editing. **Alexander Navarrete Munoz**: conceptualization, writing – review and editing, resources.

Acknowledgments

The authors thank Julia E. Bandow for fruitful discussions, access to infrastructure, and acquisition of funding (German Research Foundation, CRC1316).

Open access funding enabled and organized by Projekt DEAL.

Conflicts of Interest

The authors declare no conflicts of interest.

Data Availability Statement

The data that support the findings of this study are openly available in Research Data Repository - Science Hub Plasma at https://rdpcidat.rub.de/dataset/nanosecond-pulsed-microwave-plasma-torch-situ-h2o2-supply-path-stable-and-scalable-plasma, reference number 0f0329d3-7134-4a7b-9c56-ad1a36bb5705.

References

1. R. Ullrich, J. Nüske, K. Scheibner, J. Spantzel, and M. Hofrichter, "Novel Haloperoxidase From the Agaric Basidiomycete *Agrocybe Aegerita* Oxidizes Aryl Alcohols and Aldehydes," *Applied and Environmental Microbiology* 70 (2004): 4575–4581, https://doi.org/10.1128/aem.70.8.4575-4581.2004.

2. Y. Ni, E. Fernández-Fueyo, A. G. Baraibar, et al., "Peroxygenase-Catalyzed Oxyfunctionalization Reactions Promoted by the Complete Oxidation of Methanol," *Angewandte Chemie International Edition* 55 (2016): 798–801, https://doi.org/10.1002/anie.201507881.

3. J. Carro, A. González-Benjumea, E. Fernández-Fueyo, et al., "Modulating Fatty Acid Epoxidation vs Hydroxylation in a Fungal Peroxygenase," *ACS Catalysis* 9 (2019): 6234–6242, https://doi.org/10.1021/acscatal.9b01454.

4. Y. Wang, D. Lan, R. Durrani, and F. Hollmann, "Peroxygenases en Route to Becoming Dream Catalysts. What are the Opportunities and Challenges?," *Current Opinion in Chemical Biology* 37 (2017): 1–9, https://doi.org/10.1016/j.cbpa.2016.10.007.

5. P. George, "The Third Intermediate Compound of Horseradish Peroxidase and Hydrogen Peroxide," *Journal of Biological Chemistry* 201 (1953): 427–434, https://doi.org/10.1016/S0021-9258(18)71385-9.

6. A. Karich, K. Scheibner, R. Ullrich, and M. Hofrichter, "Exploring the Catalase Activity of Unspecific Peroxygenases and the Mechanism of Peroxide-Dependent Heme Destruction," *Journal of Molecular Catalysis B: Enzymatic* 134 (2016): 238–246, https://doi.org/10.1016/j.molcatb.2016.10.014.

7. B. O. Burek, S. Bormann, F. Hollmann, J. Z. Bloh, and D. Holtmann, "Hydrogen Peroxide Driven Biocatalysis," *Green Chemistry* 21 (2019): 3232–3249, https://doi.org/10.1039/c9gc00633h.

8. D. T. Monterrey, A. Menés-Rubio, M. Keser, D. Gonzalez-Perez, and M. Alcalde, "Unspecific Peroxygenases: The Pot of Gold at the End of the Oxyfunctionalization Rainbow?," *Current Opinion in Green and Sustainable Chemistry* 41 (2023): 100786, https://doi.org/10.1016/j.cogsc.2023.100786.

9. A. E. W. Horst, S. Bormann, J. Meyer, et al., "Electro-Enzymatic Hydroxylation of Ethylbenzene by the Evolved Unspecific Peroxygenase of *Agrocybe aegerita*," *Journal of Molecular Catalysis B: Enzymatic* 133 (2016): S137–S142, https://doi.org/10.1016/j.molcatb.2016.12.008.

10. G. V. Sayoga, V. S. Bueschler, H. Beisch, et al., "Application of the All-in-One Electrode for *In Situ* H_2O_2 Generation in Hydroxylation Catalyzed by Unspecific Peroxygenase from *Agrocybe aegerita*," *Molecular Catalysis* 547 (2023): 113325, https://doi.org/10.1016/j.mcat.2023.113325.

11. G. V. Sayoga, V. S. Bueschler, H. Beisch, et al., "Electrochemical H_2O_2 - Stat Mode as Reaction Concept to Improve the Process Performance of an Unspecific Peroxygenase," *New Biotechnology* 78 (2023): 95–104, https://doi.org/10.1016/j.nbt.2023.10.007.

12. B. O. Burek, S. R. de Boer, F. Tieves, et al., "Photoenzymatic Hydroxylation of Ethylbenzene Catalyzed by Unspecific Peroxygenase: Origin of Enzyme Inactivation and the Impact of Light Intensity and Temperature," *ChemCatChem* 11 (2019): 3093–3100, https://doi.org/10.1002/cctc.201900610.

13. X. Deng, X. Zheng, F. Jia, et al., "Unspecific Peroxygenases Immobilized on Pd-Loaded Three-Dimensional Ordered Macroporous (3DOM) Titania Photocatalyst for Photo-Enzyme Integrated Catalysis," *Applied Catalysis B: Environmental* 330 (2023): 122622, https://doi.org/10.1016/j.apcatb.2023.122622.

14. P. Püllmann, D. Homann, T. A. Karl, B. König, and M. J. Weissenborn, "Light-Controlled Biocatalysis by Unspecific Peroxygenases With Genetically Encoded Photosensitizers," *Angewandte Chemie International Edition* 62 (2023): e202307897, https://doi.org/10.1002/anie.202307897.

15. D. L. Jurković, H. Puliyalil, A. Pohar, and B. Likozar, "Plasma-Activated Methane Partial Oxidation Reaction to Oxygenate Platform Chemicals Over Fe, Mo, Pd, and Zeolite Catalysts," *International Journal of Energy Research* 43 (2019): 8085–8099, https://doi.org/10.1002/er.4806.

16. M. Borić, H. Puliyalil, U. Novak, and B. Likozar, "An Intensified Atmospheric Plasma-Based Process for the Isolation of the Chitin Biopolymer From Waste Crustacean Biomass," *Green Chemistry* 20 (2018): 1199–1204, https://doi.org/10.1039/C7GC03735J.

17. L. Wang, X. Wang, Y. Li, et al., "Breaking the Conversion-Selectivity Trade-Off Through a Plasma Reaction-Separation Coupling Process," *Chem Catalysis* 5, no. 12 (2025): 101498, https://doi.org/10.1016/j.checat.2025.101498.

18. A. Yayci, Á. G. Baraibar, M. Krewing, et al., "Plasma-Driven *In Situ* Production of Hydrogen Peroxide for Biocatalysis," *ChemSusChem* 13 (2020): 2072–2079, https://doi.org/10.1002/cssc.201903438.

19. E. Takai, K. Kitano, J. Kuwabara, and K. Shiraki, "Protein Inactivation by Low-Temperature Atmospheric Pressure Plasma in Aqueous Solution," *Plasma Processes and Polymers* 9 (2011): 77–82, https://doi.org/10.1002/ppap.201100063.

20. J.-W. Lackmann, S. Schneider, E. Edengeiser, et al., "Photons and Particles Emitted From Cold Atmospheric-Pressure Plasma Inactivate Bacteria and Biomolecules Independently and Synergistically," *Journal of The Royal Society Interface* 10 (2013): 20130591, https://doi.org/10.1098/rsif.2013.0591.

21. J.-W. Lackmann, S. Baldus, E. Steinborn, et al., "A Dielectric Barrier Discharge Terminally Inactivates RNase A by Oxidizing Sulfur-Containing Amino Acids and Breaking Structural Disulfide Bonds," *Journal of Physics D: Applied Physics* 48 (2015): 494003, https://doi.org/10.1088/0022-3727/48/49/494003.

22. A. Segat, N. N. Misra, P. J. Cullen, and N. Innocente, "Atmospheric Pressure Cold Plasma (ACP) Treatment of Whey Protein Isolate Model Solution," *IFSET* 29 (2015): 247–254, https://doi.org/10.1016/j.ifset.2015.03.014.

23. M. Krewing, B. Schubert, and J. E. Bandow, "A Dielectric Barrier Discharge Plasma Degrades Proteins to Peptides by Cleaving the Peptide Bond," *Plasma Chemistry and Plasma Processing* 40 (2020): 685–696, https://doi.org/10.1007/s11090-019-10053-2.

24. A. Yayci, T. Dirks, F. Kogelheide, et al., "Protection Strategies for Biocatalytic Proteins Under Plasma Treatment," *Journal of Physics D: Applied Physics* 54 (2021): 035204, https://doi.org/10.1088/1361-6463/abb979.

25. A. Liese and L. Hilterhaus, "Evaluation of Immobilized Enzymes for Industrial Applications," *Chemical Society Reviews* 42 (2013): 6236, https://doi.org/10.1039/c3cs35511j.

26. C. Ke, Y. Fan, F. Su, L. Xu, and Y. Yan, "Recent Advances in Enzyme Immobilization: The Role of Artificial Intelligence, Novel Nanomaterials, and Dynamic Carrier Systems," *Catalysts* 15 (2025): 571, https://doi.org/10.3390/catal15060571.

27. W. Aehle, *Enzymes in Industry: Production and Applications* (Wiley-VCH, 2007), https://doi.org/10.1002/9783527617098.

28. T. Dirks, A. Yayci, S. Klopsch, et al., "Immobilization Protects Enzymes From Plasma-Mediated Inactivation," *Journal of The Royal Society Interface* 20 (2023): 20230299, https://doi.org/10.1098/rsif.2023.0299.

29. A. Yayci, T. Dirks, F. Kogelheide, et al., "Microscale Atmospheric Pressure Plasma Jet as a Source for Plasma-Driven Biocatalysis," *ChemCatChem* 12 (2020): 5893–5897, https://doi.org/10.1002/cctc.202001225.

30. T. Winzer, D. Steuer, S. Schüttler, N. Blosczyk, J. Benedikt, and J. Golda, "RF-Driven Atmospheric-Pressure Capillary Plasma Jet in a He/O_2 Gas Mixture: Multi-Diagnostic Approach to Energy Transport," *Journal of Applied Physics* 132 (2022): 183301, https://doi.org/10.1063/5.0110252.

31. T. Dirks, D. Stoesser, S. Schüttler, F. Hollmann, J. Golda, and J. E. Bandow, "The Atmospheric Pressure Capillary Plasma Jet is Well-Suited to Supply H_2O_2 for Plasma-Driven Biocatalysis," *ChemistryOpen* 22 (2025): e2500057, https://doi.org/10.1002/open.202500057.

32. S. Schüttler, L. Jolmes, E. Jeß, K. Tschulik, and J. Golda, "Validation of *In Situ* Diagnostics for the Detection of OH and H_2O_2 in Liquids Treated by a Humid Atmospheric Pressure Plasma Jet," *Plasma Processes and Polymers* 21 (2024): 2300079, https://doi.org/10.1002/ppap.202300079.

33. F. Thevenet, J. Couble, M. Brandhorst, et al., "Synthesis of Hydrogen Peroxide Using Dielectric Barrier Discharge Associated With Fibrous Materials," *Plasma Chemistry and Plasma Processing* 30 (2010): 489–502, https://doi.org/10.1007/s11090-010-9234-7.

34. R. Snoeckx and A. Bogaerts, "Plasma Technology-A Novel Solution for CO_2 Conversion?," *Chemical Society Reviews* 46 (2017): 5805–5863, https://doi.org/10.1039/c6cs00066e.

35. Z. Jie, C. Liu, S. Huang, and G. Zhang, "Mechanisms of Gas Temperature Variation of the Atmospheric Microwave Plasma Torch," *Journal of Applied Physics* 129 (2021): 233302, https://doi.org/10.1063/5.0049620.

36. S. N. Andreev, L. M. Apasheva, M. K. Ashurov, et al., "Production of Pure Hydrogen Peroxide Solutions in Water Activated by the Plasma of Electrodeless Microwave Discharge and Their Application to Control Plant Growth," *Physics of Wave Phenomena* 27 (2019): 145–148, https://doi.org/10.3103/s1541308x19020109.

37. S. Soldatov, G. Link, L. Silberer, et al., "Time-Resolved Optical Emission Spectroscopy Reveals Nonequilibrium Conditions for CO_2 Splitting in Atmospheric Plasma Sustained with Ultrafast Microwave Pulsation," *ACS Energy Letters* 6 (2021): 124–130, https://doi.org/10.1021/acsenergylett.0c01983.

38. M. S. Hernandez, Y. Mikolaiczyk, S. Soldatov, et al., "Overcoming Thermal Degradation During Continuous Conversion of Water Into Hydrogen Peroxide in a Flexible Plasma Reactor," *Journal of the American Chemical Society* 148, no. 10 (2026): 10378–10387, https://doi.org/10.1021/jacs.5c14829.

39. B. R. Allen, M. Charles, and R. W. Coughlin, "Fluidized-Bed Immobilized-Enzyme Reactor for the Hydrolysis of Cornstarch to Glucose," *Biotechnology and Bioengineering* 21 (1979): 689–706, https://doi.org/10.1002/bit.260210413.

40. A. Bódalo, J. L. Gómez, E. Gómez, J. Bastida, and M. F. Máximo, "Fluidized Bed Reactors Operating With Immobilized Enzyme Systems: Design Model and Its Experimental Verification," *Enzyme and Microbial*

Technology 17 (1995): 915–922, https://doi.org/10.1016/0141-0229(94)00125-b.

41. M. V. C. da Silva, A. B. S. Rangel, L. G. Aguiar, H. F. de Castro, and L. de Freitas, "Continuous Enzymatic Synthesis of 2-Ethylhexyl Oleate in a Fluidized Bed Reactor: Operating Conditions, Hydrodynamics, and Mathematical Modeling," *Industrial & Engineering Chemistry Research* 59 (2020): 19522–19530, https://doi.org/10.1021/acs.iecr.0c03504.

42. L.-E. Meyer, B. F. Hauge, T. M. Kvorning, P. de Santis, and S. Kara, "Continuous Oxyfunctionalizations Catalyzed by Unspecific Peroxygenase," *Catalysis Science & Technology* 12 (2022): 6473–6485, https://doi.org/10.1039/D2CY00650B.

43. G. Eisenberg, "Colorimetric Determination of Hydrogen Peroxide," *Industrial & Engineering Chemistry Analytical Edition* 15 (1943): 327–328, https://doi.org/10.1021/i560117a011.

44. H. I. A. Qazi, Q.-Y. Nie, H.-P. Li, X.-F. Zhang, and C.-Y. Bao, "Comparison of Electrical and Optical Characteristics in Gas-Phase and Gas-Liquid Phase Discharges," *Physics of Plasmas* 22 (2015): 123512, https://doi.org/10.1063/1.4937779.

45. P. Molina-Espeja, S. Ma, D. M. Mate, R. Ludwig, and M. Alcalde, "Tandem-Yeast Expression System for Engineering and Producing Unspecific Peroxygenase," *Enzyme and Microbial Technology* 73 (2015): 29–33, https://doi.org/10.1016/j.enzmictec.2015.03.004.

Supporting Information

Additional supporting information can be found online in the Supporting Information section.

Supporting File 1: cctc71023-sup-0001-SuppMat.docx.